Point Mutations in TbpA Abrogate Human-Transferrin Binding in *Neisseria gonorrhoeae*

Ashley Greenawalt,[a] Julie Stoudenmire,[a] Karl Lundquist,[b,c,d] Nicholas Noinaj,[b,c,d] James C. Gumbart,[e] and Cynthia Nau Cornelissen[a*]

[a]Center for Translational Immunology, Institute for Biomedical Sciences, Georgia State University, Atlanta GA, 30303.

[b]Markey Center for Structural Biology, Department of Biological Science, Purdue University, West Lafayette, Indiana, USA

[c]Purdue Institute of Inflammation, Immunology and Infectious Disease, Purdue University, West Lafayette, Indiana, USA

[d]Department of Biological Sciences, Purdue University, West Lafayette, Indiana, USA

[e] School of Physics, Georgia Institute of Technology, Atlanta, GA, 30332

*To whom correspondence should be addressed: Cynthia Nau Cornelissen, Georgia State University, Atlanta GA 30303. ccornelissen@gsu.edu. Tel. (404)-413-6680

Keywords: TonB-dependent transporter, Transferrin Binding Protein A, Transferrin, Site-directed mutagenesis, *N. gonorrhoeae, N. meningitidis*

Running title: Mutagenesis of gonococcal TbpA

Abstract

TonB-dependent transporters (TDTs) are essential proteins for metal acquisition, an important step in growth and pathogenesis for many pathogens, including *Neisseria gonorrhoeae*, the causative agent for gonorrhea. There is currently no available vaccine for gonorrhea; TDTs are being investigated as vaccine candidates because they are highly conserved and expressed *in vivo*. TbpA is an essential virulence factor in the initiation of experimental infection in human males and functions by acquiring iron upon binding to host transferrin (hTf). The loop 3 helix (L3H) is a helix finger that inserts into the hTf C-lobe and is required for hTf binding and subsequent iron acquisition. This study identified and characterized the first TbpA single point substitutions resulting in significantly decreased hTf binding and iron acquisition, suggesting that the helix structure is more important than charge for hTf binding and utilization. The *tbpA* D355P *tbpB*- and *tbpA A356P tbpB*- mutants demonstrated significantly reduced hTf binding and impaired iron uptake from Fe-loaded hTf; however, only *tbpA A356P tbpB*- was able to grow when hTf was the sole source of iron. Expression of *tbpB* was able to restore function in all *tbpA* mutants. These results implicate both D355 and A356 in the key binding, extraction and uptake functions of gonococcal TbpA.

41 **Introduction**

42 *Neisseria gonorrhoeae* is the human-specific pathogen that causes the sexually-
43 transmitted infection, gonorrhea. The World Health Organization (WHO) reported 87 million
44 new cases globally in 2016 (1), and the Centers for Disease Control and Prevention (CDC)
45 estimates that approximately 1.6 million new cases occurred in 2018 in the United States alone
46 (2). Uncomplicated gonorrhea presents as urethritis in men and cervicitis in women (3-6). An
47 estimated 80% of gonococcal infections in women are asymptomatic (3, 7). Asymptomatic
48 cases left untreated allow for gonococcal infection to ascend upwards in the reproductive tract
49 and cause more severe secondary sequalae, such as pelvic inflammatory disease, ectopic
50 pregnancy, and infertility (3). Previous gonococcal infection does not provide protective
51 immunity (5, 8, 9), and there has been a rise in the incidence of antimicrobial resistance among
52 gonococcal isolates (1, 10-16). Reports to the WHO in 2018 indicated that 7 out of 65 countries
53 reported isolating gonococcal strains with decreased susceptibility or resistance to extended-
54 spectrum cephalosporins (10). Drastic increases in antimicrobial resistance, including resistance
55 to azithromycin, caused the CDC to modify recommendations for treatment as of late 2020;
56 uncomplicated gonococcal infection should currently be treated with monotherapy of
57 ceftriaxone without additional oral azithromycin (17). Availability of effective therapeutics have
58 dwindled to the point that researchers are analyzing older antibiotics as potential alternative
59 treatments against gonorrhea infection (15). The widespread prevalence of gonococcal
60 infection, increasing incidence of antibiotic resistance, and lack of protective immunity add
61 urgency to the development of an effective gonococcal vaccine.

62 Many of the neisserial outer membrane proteins, such as the Opas and pilin, are subject
63 to high-frequency antigenic variation (18-21), allowing the gonococcus to effectively
64 camouflage itself from an adaptive immune response. This genetic adaptability has presented
65 quite a challenge in vaccine development. TonB-dependent metal transporters (TDTs) have
66 been the focus of several vaccine studies (20, 22-28). TDTs are well-suited vaccine candidates
67 because they are highly conserved, present in all pathogenic *Neisseria* (29), expressed *in vivo*
68 (30), and many are not subject to high-frequency antigenic variation (20, 31). The importance of
69 TbpAB in gonococcal infection has been demonstrated in a human male infection study, where
70 a *tbpAB* double knockout mutant was unable to elicit signs or symptoms of urethritis in human
71 male volunteers (4). The mechanism for iron piracy through hTf interaction with TbpA is crucial
72 to understand as TbpA is being evaluated as a potential vaccine and therapeutic target.
73 *Neisseria* species can acquire iron through the TDT transferrin-binding protein A (TbpA)
74 (25, 32). With the help of the lipoprotein TbpB, human transferrin (hTf) binds to TbpA, and iron
75 is internalized in a TonB-dependent mechanism powered by proton-motive force (29, 32-35).
76 TbpA is required for iron acquisition from hTf (36, 37), and TbpB increases the efficiency of hTf-
77 binding (38, 39). TbpA binds both apo- and saturated hTf with similar affinity, but TbpB
78 preferentially binds to Fe-saturated hTf (40, 41).
79 The exact interaction between TbpA and hTf is still being elucidated. The co-crystal
80 structure of TbpA and bound hTf demonstrates a helix finger in loop 3 (L3H) that projects into
81 the cleft of the hTf C-lobe (29). TbpA exclusively interacts with the C-lobe for hTf acquisition,
82 hinting at the importance of the L3H interaction in iron extraction (29). Three pH-sensing
83 residues (K534, R632, and D634) reside in the C-lobe cleft to store iron (25, 29). Upon hTf

84 binding, TbpA L3H, which contains a positive charge at the penultimate residue (K359), is
85 hypothesized to interact with the hTf C-lobe D634 to cause a conformational change in the C-
86 lobe, resulting in the release and subsequent internalization of iron (25, 42). Mutation of D634A
87 increased iron release by 83 fold, indicating that D634 neutralizes the positive charges of K359
88 and R632 (43).Upon hTf binding, the L3H K359 residue is inserted near the C-lobe D634, which
89 causes a charge repulsion to release iron (44). An HA epitope insertion into the extracellular
90 loop 3 (L3) and deletion of the L3H were both disruptive enough to abrogate hTf binding and
91 iron acquisition, demonstrating that the L3H is essential for hTf binding and iron acquisition
92 from hTf (25, 45). Alanine or opposite charge amino acid substitutions in the L3H failed to
93 significantly abrogate hTf binding (25).
94 The current study aims to extend previous TbpA structure-function analyses by
95 generating proline-substitution mutants in the TbpA L3H. The structure of proline contains a
96 ring, which is predicted to disrupt the helix motif. Characterization of 16 proline substitution
97 mutants for hTf binding, iron uptake from hTf, and growth using hTf as the sole iron source
98 helped to elucidate the details of the interaction between the L3H and hTf. Understanding the
99 mechanism for binding is essential in the development of therapeutics and vaccines. Drugs
100 could be developed to block hTf binding for treatment of infection (42). TbpA mutants unable
101 to bind hTf with minimal protein conformational changes compared to the wild-type (WT)
102 protein could be tested for immunogenicity similar to protection studies using nonbinding TbpB
103 and factor H binding protein (fHbp) as vaccine antigens (28, 46). Molecular dynamics (MD)
104 simulations were utilized to predict protein conformational changes in lieu of an available

105 crystal structure. In this study, two mutants with single proline-substitutions in TbpA

106 demonstrated significantly reduced hTf binding and iron internalization.

107

108 **Results**

109 **The TbpA L3H sequence is well conserved at the amino terminus, but residues are more**

110 **variable at the carboxy-terminal end.**

111 TbpA from *N. meningitidis* strain K454 has been previously crystalized (29) and shares

112 94% sequence identity with TbpA from *N. gonorrhoeae* strain FA19 (32). Using this similarity,

113 we generated a homology model for TbpA from gonococcal strain FA19, which is shown in **FIG**

114 **1.** Key components of the TbpA structure include the outer-membrane embedded beta-barrel

115 motif; key hTf-interacting region, the L3H; and the TonB-interacting region, the plug domain

116 **(FIG 1A and FIG 1C, yellow, green, and cyan respectively).** A closer look at the L3H **(FIG 1B)**

117 shows the key residues that were mutated in this study in order to test structure/function

118 relationships. **FIG 1C** shows TbpA from a top-down perspective to demonstrate the location of

119 the plug domain. Both the FA19 model and the K454 TbpA structure share the L3H, previously

120 shown to be essential for hTf binding (25, 29, 45). Interestingly, the helical structure is well

121 conserved, despite considerable variability at the carboxy-terminal end, the region that

122 interacts with the iron in hTf during iron acquisition **(FIG 2A).** In an attempt to identify residues

123 critical for hTf binding, site-directed mutagenesis was conducted on several residues within the

124 TbpA L3H region from D355 to Q360, substituting each residue with a proline **(FIG 2B).**

125 **Mutagenized TbpA was surface exposed despite proline substitutions in the L3H.**

126 A previous study characterized several FA19 *tbpA* L3H point mutants and did not

127 identify any single residue that completely abrogated hTf binding (25). The current study

128 extends the previous findings by substituting residues within the L3H with proline, which are

129 proposed to be more impactful on the secondary structure of the helix. To evaluate expression

130 of TbpA in each mutant, strains were grown under iron-stressed conditions; whole-cell lysates
131 were prepared, run on SDS-PAGE, and transferred to nitrocellulose for western blotting using a
132 polyclonal anti-TbpA antibody **(S1).** The western blot analysis showed approximately equivalent
133 levels of TbpA protein produced by all mutants. Because mutagenesis has the potential to
134 disrupt 3D protein conformation and localization to the outer membrane, each strain was
135 evaluated for proper surface exposure of TbpA using protease digestion. Each gonococcal strain
136 was grown under iron-stressed conditions, then subjected to a time course of trypsin digestion
137 before whole-cell lysates were collected for western blot analysis **(S2).** As the cells were
138 exposed to trypsin, full-length TbpA, approximately 100 kDa, was cleaved, producing 95 kDa
139 and 55 kDa degradation products, as previously described (25, 40). Each mutant showed a
140 similar pattern compared to FA19 (WT). Taken together, these data suggest that the mutations
141 did not disrupt TbpA production or wild-type surface exposure.

142 **Selected mutants, containing proline substitutions in L3H, are deficient in hTf binding.**

143 Proline-substitution mutants were evaluated for their ability to bind hTf in whole-cell
144 binding assays. Since TbpB expressed by whole *N. gonorrhoeae* is also capable of binding to hTf,
145 only *tbpB*- strains were used for the hTf-binding analyses. Whole-cell ELISAs of strains lacking
146 *tbpB* were conducted using HRP-conjugated hTf as the ligand **(FIG 3).** In these experiments,
147 FA6905 (*tbpA+/tbpB*-) was used as a positive control **(FIG 3, WT)** and two negative controls
148 were used: FA6815 **(*tbpA-/tbpB-*, FIG 3, Neg)** and competitive inhibition **(FIG 3, WT w/Comp**
149 **and Neg w/Comp)** conditions, which were generated by adding 100x excess unlabeled apo-hTf
150 to both FA6905 and FA6815. A previous study showed that a mutant with a deletion of the L3H
151 binds hTf at about 9% the levels of a strain expressing WT TbpA, and mutants expressing *tbpA*

152 with alanine or charge-change point mutations reduced hTf binding to approximately 40-80% of
153 WT FA6905 (*tbpA+/tbpB-*) levels (25). The current study found significantly reduced hTf binding
154 in almost every *tbpA* mutant **(FIG 3).** Significantly reduced hTf binding levels in mutants ranged
155 from approximately 14-58% of FA6905 (*tbpA+/tbpB-*). Two mutants in particular, *tbpA* D355P
156 *tbpB-* and *tbpA* A356P *tbpB-* (approximately 14% and 18% of WT HRP-hTf binding, respectively)
157 showed the lowest levels of HRP-hTf binding of all tested mutants; the hTf-binding levels in the
158 *tbpA* D355P *tbpB-* and *tbpA* A356P *tbpB-* mutants were not statistically different from the
159 negative controls **(FIG 3)**.

160 **L3H proline mutants in a *tbpB-* background are deficient in iron internalization from hTf.**

161 Mutants with decreased hTf binding were hypothesized to demonstrate diminished
162 levels of internalized iron. Internal iron pools were measured using inductively coupled plasma
163 mass spectrometry (ICP-MS) in the WT *tbpA* strain and proline-substitution mutants. In the
164 *tbpB-* background, the *tbpA* D355P, A356P, N357P, Q358P, and double K359P Q360P mutants
165 demonstrated statistically reduced levels of iron internalization compared to the WT *tbpA*
166 strain (FA19) **(FIG 4)**. These same mutants in a *tbpB+* background did not demonstrate
167 statistically different levels of iron internalization compared to the WT *tbpA* strain, suggesting
168 that expression of TbpB is able to compensate for these proline substitutions in TbpA **(FIG 4)**.
169 These data also indicate that the mutagenized TbpA proteins are not significantly impaired in
170 membrane localization or structure, consistent with data described above.

171

172

173 **Several mutants, with proline substitutions in the L3H of *tbpA* in a *tbpB*- background, are**
174 **unable to grow if hTf is the sole source of iron.**
175 In a previous study, only the L3H deletion mutant showed any defect in growth when
176 employing hTf as a sole iron source, regardless of the presence of *tbpB* (25). Using the same
177 methodology, the growth phenotype of the *tbpA* mutants was characterized by plating mutant
178 gonococcal strains onto solid media providing hTf as the sole source of iron. Approximately
179 equal inocula were applied to Fe-deficient CDM agarose plates supplemented with 30% Fe-
180 saturated hTf as the sole iron source **(FIG 5)**. FA19 (*tbpA+/tbpB+*) and FA6905 (*tbpA+/tbpB-*)
181 served as positive controls and FA6747 (*tbpA-/tbpB+*) and FA6815 (*tbpA-/tbpB-*) served as
182 negative controls. As seen previously (25), all *tbpB+* strains were able to grow like the WT *tbpA*
183 strain **(FIG 5B).** Both the *tbpA* D355P and the quadruple *tbpA* N357P/Q358P/K359P/Q360P
184 mutants in a *tbpB-* background were unable to grow on solid CDM with hTf as the sole source of
185 iron **(FIG 5A)**.
186 To assess the growth defect of the *tbpA* D355P *tbpB-* mutant further, a liquid CDM
187 growth assay was developed. Iron-starved cells were transferred to a 96-well plate and
188 supplemented with 5 µM 30% iron-saturated hTf and 5 µM Desferal to chelate free iron, and
189 the growth was monitored over 24 hours. The *tbpA* D355P *tbpB-* strain demonstrated
190 essentially no growth in the liquid growth assay **(FIG 6)**.
191 **The *tbpA* D355P *tbpB*- mutant demonstrates reduced hTf binding in serum.**
192 To assess if the binding deficiency in the *tbpA* D355P *tbpB-* mutant could be replicated in
193 a more biologically relevant environment, three samples of human serum were pooled and
194 used as a source of hTf to assess hTf-TbpA binding on whole cells. FA6905 (*tbpA+/tbpB-*) served

195 as a positive control for hTf binding, and FA6815 (*tbpA-/tbpB-*) served as a negative control for
196 hTf binding. The controls and the *tbpA* D355P *tbpB-* strain were grown in Fe-deplete liquid
197 CDM. Whole cells were blocked with BSA prior to adding hTf or pooled human serum and after
198 a 20-minute incubation, lysates were collected for western blot analysis **(FIG 7)**. Approximately
199 equivalent levels of TbpA were detected in the *tbpA* D355P *tbpB-* strains compared to FA6905
200 (*tbpA+/tbpB-*), but reduced binding was detected in the case of hTf alone and hTf in the context
201 of serum using the *tbpA* D355P *tbpB-* mutant. The small amount of background binding in
202 FA6815 (*tbpA-/tbpB-*) suggests that there may be components in the serum that allow hTf to
203 interact with the gonococcus in a TbpAB-independent mechanism.

204 **Molecular dynamics simulations suggest that D355P mutagenesis is disruptive to the TbpA L2**
205 **and L3 structures, but not to L5.**

206 Because there is no experimentally determined structure of the D355P mutant, we
207 instead used molecular dynamics simulations to model its effects on the structure and
208 dynamics of L3H and the interactions between TbpA and hTf. Molecular dynamics (MD) is a
209 mature approach that provides atomistic-level insight into the microsecond-scale dynamics of
210 proteins in native-like environments with typically high qualitative and quantitative agreement
211 with experimental measurements (Hollingsworth2018). Here, MD simulations were performed
212 on four systems: WT TbpA, WT TbpA +hTf, D355P TbpA, D355P TbpA + hTf; in all systems, the
213 protein was embedded in a realistic species-specific outer-membrane model and solvated with
214 water and ions (see Methods). Two replicas were run for each system in order to improve the
215 reliability of our observations (Knapp2018). The L3H begins at residue 351 and ends at 361, as
216 shown by the α-helix (H, orange) in **FIG 8**. The presence of hTf stabilized the α-helix secondary

217 structure, as demonstrated by fewer interruptions of the α-helix in WT TbpA+ hTf **(FIG 8B)**
218 compared to WT TbpA **(FIG 8A)**. The α-helix structure of the L3H was interrupted by β-turns (T,
219 blue) after D355P mutagenesis **(FIG 8C)**; however, the presence of hTf appeared to be
220 moderately stabilizing to the helical structure despite D355P mutagenesis **(FIG 8D)**. To assess
221 whether the mutation in the L3H impacted the overall structure of the protein, two wild-type
222 loops were assessed for their structure compared to WT TbpA. The predicted secondary
223 structure of extracellular L2 demonstrated some variation between residues 262 and 276 **(FIGS**
224 **S4, S5)**; however, the predicted secondary structure of the extracellular L5 remained highly
225 conserved **(FIGS S6, S7)**.
226 We also measured the root-mean-square deviation (RMSD) for TbpA L3H over time for
227 each simulated system and replica. This metric illustrates how much the region diverges from
228 the original structure over time after being superimposed. The RMSD values measured here
229 demonstrate that there is more distance between TbpA L3H in TbpA D355P and TbpA D355P
230 +hTf compared to WT TbpA and WT TbpA +hTf **(FIG 9)**. Consistent with **FIG 8**, the RMSD plots
231 also demonstrated that the presence of hTf is more stabilizing to secondary structure **(FIG 9)**.
232 The number of hydrogen bonds between TbpA and hTf were also tracked for the WT and D355P
233 mutant systems **(FIG 10)**. We find that for one of the two replicas, the number of hydrogen
234 bonds in the D355P mutant drop precipitously after ~200 ns, from ~11 to 6. In contrast, both
235 WT replicas maintain a similar number of hydrogen bonds (~10-12) throughout the trajectories.
236 **Discussion**
237 Prior to this study, no TbpA point mutation has been observed to completely abrogate
238 hTf binding. The generation of such mutants was facilitated by the availability of the 3D crystal

239 structure of TbpA from *N. meningitidis* (K454) bound to hTf (25, 47). Because the TbpA
240 sequence from gonococcal strain FA19 shares 94% sequence identity with the meningococcal
241 K454 strain, important structural inferences can be made to identify crucial binding domains
242 (25). Initially, the K359 and Q360 residues were predicted to be key hTf-interacting and binding
243 partners based on their charge and proximity to the C-lobe of hTf (25). The previous
244 mutagenesis study demonstrates that alanine or opposite charge point substitutions are
245 insufficient in abolishing hTf binding and TbpA function. In the previous study, the most
246 substantial decrease in hTf-binding was observed with substitution of residue 360Q to a
247 negative charge, followed by substitution of residue 359K with the opposite or no charge (25).
248 The high conservation of L3H secondary structure among *Neisseria sp.* and the data from this
249 study suggest that the structure of the helix may be more important for function than the
250 charges of L3H residues (48). A recent study provides evidence supporting the role of the helix
251 finger using MD simulations demonstrated that the L3H is shifted downward, impeding hTf
252 binding (42). Additionally, L5 and L8 shifted closer, suggesting a "closed" state to prevent hTf
253 binding (42).

254 Both *tbpA* D355P *tbpB*- and *tbpA* A356P *tbpB*- mutants showed the lowest levels of hTf
255 binding of all tested mutants compared to WT. Similarly, both the *tbpA* D355P *tbpB*- and *tbpA*
256 A356P *tbpB*- mutants demonstrated significantly reduced iron internalization compared to WT.
257 Together, these findings suggest that proline substitutions in the beginning of the L3H are more
258 disruptive to the structure and function than proline substitutions near the end of the L3H.

259 Interestingly, the *tbpA* A356P *tbpB*- mutant was able to grow with hTf as the sole source
260 of iron, whereas the *tbpA* D355P *tbpB*- mutant could not. Without a functional TbpA, growth

261 using hTf as the sole iron source would be impossible. These data suggest that the *tbpA* A356P
262 *tbpB*- mutant is able to overcome the decrease in hTf binding and iron internalization by
263 obtaining iron elsewhere to grow. All strains were grown on Desferal plates to ensure that iron
264 stores in the strains would not influence the results; however, it is possible that there were
265 some residual internal iron stores that allowed for growth. Quantification of iron via ICP-MS is
266 very sensitive; therefore, trace iron levels could account for the variation observed.

267 Iron-internalization levels from all proline substitution *tbpA* L3H *tbpB*- mutants were
268 significantly reduced compared to WT FA6905 (*tbpA+/tbpB-)*, suggesting that despite some hTf-
269 binding, there is still a defect in iron internalization. These results are consistent with a previous
270 study demonstrating that high-affinity hTf binding to TbpA loops L4, L5, and L8 is required for
271 iron internalization (49). Deletion of TbpA extracellular L4 and L5 completely abolishes hTf
272 binding, whereas deletion of L8 inhibits hTf binding by 10-fold (49). In all three deletions, iron
273 internalization is abolished (49). These findings are consistent with the results of this study:
274 while hTf binding was not completely abrogated in each *tbpA* L3H *tbpB*- mutants, most mutants
275 demonstrated reduced iron internalization.

276 As observed previously (25, 45), the expression of *tbpB* rescues TbpA function despite a
277 decrease in TbpA-hTf binding in each *tbpA* mutant used in this study. Two mutants (the *tbpA*
278 D355P *tbpB*- mutant and the quadruple *tbpA* D355P, A356P, N357P, 358P *tbpB*- mutant) did not
279 grow with hTf as the sole source of iron; however, expression of *tbpB* restored function. The
280 ability for *tbpB* to restore function suggests that inhibition of hTf binding or iron internalization
281 is likely caused by small conformational changes small enough not to alter overall protein
282 conformation.

283 Nonbinding mutants for use in a vaccine should maintain the overall conformation of
284 the WT protein, to stimulate the immune response and elicit antibodies that recognize WT
285 epitopes. To evaluate how D355P L3H proline substitution may affect overall protein
286 conformation, the predicted secondary structures of extracellular L2 and L5 were monitored
287 over the course of 500-ns simulations. Both L2 and L5 have a demonstrated role in hTf binding
288 (45, 49). The simulation results suggest that D335P mutagenesis affects the secondary structure
289 of the L3H region and a short region in the L2, but otherwise the overall secondary structures of
290 L2, L3, and L5 is maintained. Thus, the overall 3D conformation of the protein is predicted to be
291 similar to WT (45). MD simulation provides valuable insight in the hTf-TbpA interaction. The
292 data from this study suggests that the TbpA D355P mutation is destabilizing to the α-helical
293 structure of the L3H; furthermore, hydrogen bonding between TbpA and hTf is notably reduced
294 in one of the two replicates of the TbpA D355P mutant when started in the hTf-bound state
295 (**FIG 10**). Recent evidence suggests that TbpA extracellular L5 and L8 flex to an "open" state,
296 opening a pocket for hTf to bind (42). This implies that the hTf C-lobe is in an open and
297 unbound state as a result of the L3H D355P substitution. L3 is sandwiched between L2 and L5,
298 which are the longest extracellular loops (50). In variants with higher levels of hTf binding but
299 low levels of iron internalization, it is possible that L3H point mutations cause a small but
300 impactful change to the TbpA structure that allows for poor hTf binding or possible
301 downstream conformational changes, such as blocking the β-barrel pore or the TonB-box,
302 which is responsible for transporting iron into the β-barrel (51).
303 Proper WT TbpA function is observed in *tbpA* L3H mutants with proper *tbpB* expression
304 in previous studies with the exception of the L3H deletion mutant (25, 45, 49). Because TbpB

305 can bind to hTf and facilitate iron transfer, incorporation of TbpB in a vaccine will also require
306 mutagenesis or modification to inhibit binding to hTf, as binding to host proteins has been
307 shown to inhibit a robust immune response (23, 28). Because TbpB is more immunogenic and
308 sequence variable, and TbpA is less immunogenic but shares more sequence conservation
309 among strains, a combination of both Tbps is predicted to enhance protection and the immune
310 response (30, 52, 53). Ideally, non-host binding variants of both Tbps would be included in a
311 vaccine cocktail to increase immunogenicity and protection. As more TDTs are characterized,
312 nonbinding mutants can be included in this vaccine cocktail to enhance protection and
313 immunogenicity.

314 The ability of a vaccine antigen to bind to host proteins is hypothesized to inhibit the
315 development of a robust immune response and may explain the weak immunogenicity of WT
316 TbpA, WT TbpB, and WT fHbp (25, 29, 31, 54). Generation of mutants unable to bind host
317 ligands has already been shown to be a viable option in creating a superior vaccine candidate
318 using TbpB and fHbp (23, 28, 46, 55). This is the first study to identify a point mutant in *tbpA*
319 that completely abrogates both binding and growth functions. Future studies will focus on
320 elucidating the interaction between the L3H and iron extraction from hTf using structural
321 analysis and comparing the immunization potential using the TbpA D355P and TbpA A356P
322 variants in a human transferrin transgenic mouse model.
323

324 **Materials and Methods**

325 **Strains, plasmids, and media.** All primers and plasmids used in the study are described in Table
326 1. Site-directed mutagenesis started with the plasmid pUNCH755 (38). All strains utilized in this
327 study are described in Table 2. Plasmids were propagated in *Escherichia coli* Top10 (Invitrogen),
328 *E. coli* XL-10 Gold cells (Agilent Technologies), or NEB 5-alpha *E. coli* (New England BioLabs). *E.*
329 *coli* was cultured in Luria-Bertani broth (10 g tryptone, 5 g NaCl, 5 g yeast extract in 1 L of
330 water) in the presence of ampicillin/carbenicillin (100 µg/mL) or chloramphenicol (34 µg/mL),
331 where appropriate.

332 **Site-directed mutagenesis.** Site-directed mutagenesis was performed using the QuikChange II
333 Site-Directed Mutagenesis Kit (Agilent Technologies Cat: 200523) or the Q5 Site-Directed
334 Mutagenesis Kit (New England BioLabs Cat: E0552S) per manufacturer's instructions. NEB 5-
335 alpha competent *E. coli* or XL10 Ultracompetent Gold *E.* coli were transformed with
336 mutagenized pUNCH755. First, a StuI restriction site was inserted downstream of the *tbpA* L3H
337 region in pUNCH755. The StuI insertion was used to identify gonococcal transformants that
338 retained WT *tbpA* sequence. Polymerase chain reaction (PCR) was used to amplify *tbpA* from
339 transformant DNA and PCR products were digested with StuI; WT *tbpA* does not contain the
340 StuI site, but site-directed mutants retained the site. Following StuI restriction site insertion,
341 proline mutations were directed to the L3H region of *tbpA* between D355 and Q360 as
342 described in Table S1. Primers and plasmids are further described in Table 1. Sequences of
343 mutated plasmids were confirmed before transformation into gonococcal strain FA19. As
344 described previously, gonococcal transformation with one plasmid yielded two genotypes:
345 *tbpA+/tbpB+* and *tbpA+/tbpB-* (25). Mutated FA19 strains were single-colony purified and then

346 characterized as either *tbpB+* or *tbpB-* by PCR, amplifying the wild-type or mutagenized *tbpB*
347 gene.
348 **Gonococcal growth.** Gonococci were propagated using GC medium base (GCB; Difco) with
349 Kellogg's Supplement I (56) and 12 µM $Fe(NO_3)_3$ at 35-37°C with 5% atmospheric CO_2. To
350 provide selection of gonococcal transformants, 1 µg/mL chloramphenicol was added to GCB
351 agar plates. Gonococcal strains were iron-stressed with 10 µM deferoxamine mesylate
352 (Desferal) on GCB agar plates or cultured from GCB plates into liquid chemically-defined media
353 (CDM) pretreated with Chelex 100 (Bio-Rad) to remove excess metals as described previously
354 (57).
355 **Homology modeling of TbpA and alignment of the L3H.** The homology model of TbpA from
356 strain FA19 was generated based on the known structure of TbpA from *N. meningitidis* strain
357 K454. Phyre 2.0 was used to generate the PDB file, and PyMOL was used to generate FIG 1.
358 ESPript 3.0 was used to generate the multiple strain alignment and secondary structure
359 prediction of TbpA L3H as previously described (58). GenBank Accession Numbers include the
360 following: *N. gonorrhoeae* FA19: EEZ46093.1; *N. gonorrhoeae* FA1090: WP_010951283.1; *N.*
361 *gonorrhoeae* DG12: EFE04786.1; *N. meningitidis* K454: AAF81744.1.
362 **Western blotting.** Gonococcal strains were grown under iron stressed conditions using CDM, as
363 described above. Cells were harvested 3-4 hours after culturing at 36°C with 5% CO_2 to a
364 standardized density. Pellets were standardized by weight and lysed in 2x Laemmli solubilizing
365 buffer (Bio-Rad) supplemented with 5% β-mercaptoethanol. Whole-cell lysates were boiled for
366 10 minutes. A total of 10 µL of lysate per sample was loaded onto a 7.5% SDS-PAGE. Proteins
367 were transferred to a 0.45 µM nitrocellulose membrane. Uniform protein loading was

368 confirmed via Ponceau S staining after transfer and prior to blocking. Blots were blocked with
369 5% Bovine Serum Albumin (BSA) in high-salt TBS (HS-TBS) (20 mM Tris, 500 mM NaCl [pH 7.5],
370 0.05% Tween20) and probed for TbpA using polyclonal rabbit serum against full-length TbpA
371 (36). Goat anti-rabbit IgG conjugated to horseradish peroxidase (HRP; Bio-Rad) or rabbit anti-
372 goat IgG HRP (Bio-Rad) were used as secondary antibodies. Goat anti-hTf (Sigma) was used to
373 detect hTf. OPTI-4CN (Bio-Rad) or West Femto (Thermo) were used as substrates per
374 manufacturers' recommendations. Images were acquired using a Bio-Rad Chemidoc System.
375 **Protease accessibility assay.** Trypsin digest assays were completed as previously described (40).
376 Briefly, gonococcal cells were grown in liquid CDM as described above, diluted to a standardized
377 density, and grown for an additional 3-4 hours at 36°C with 5% CO_2. Whole, iron-stressed
378 gonococci were treated with 2.5 µg trypsin (Sigma) per mL of culture for 0, 10, 20, or 30 minutes
379 at 36°C with 5% CO_2. Reactions were stopped by addition of 0.6 trypsin-inhibiting units of
380 aprotinin (Sigma). Whole-cell lysates were collected and subjected to western blotting for TbpA
381 detection, as described above.
382 **hTf-binding ELISA**. hTf (Sigma) was prepared as previously described (59). Strains were iron-
383 starved on GCB agar plates supplemented with 12.5 µM Desferal overnight to induce TbpA
384 expression. MaxiSorp microtiter plates (Nunc), pre-treated with 200 µL 0.01% poly-lysine
385 (Sigma), were inoculated with whole gonococcal cells scraped from GCB Desferal plates. Cells
386 were resuspended to a standardized density of 1.0 OD_{600} and then 100 µL per strain was
387 inoculated into triplicate wells and allowed to incubate for 1 hour at room temperature.
388 Unbound cells in the suspension were removed and plates were blocked with 200 µL 3% BSA in
389 Phosphate Buffered-Saline (PBS) for 1 hour at room temperature. Blocking was followed by the

390 addition of 1 µg/mL HRP-conjugated hTF (Jackson ImmunoResearch) dissolved in 1x PBS also
391 containing 3% BSA for 1 hour at room temperature. To show specificity, 100 µg/mL apo-hTF
392 was added as a competitor to HRP-hTf Comp wells. Wells were washed 3 times in 200 µL 1x PBS
393 using a plate washer (BioTek). Colorimetric 1-Slow-step TMB ELISA Substrate solution (Thermo)
394 was applied until sufficient color change was observed, and the reaction was quenched with
395 100 µL 1.8 N H_2SO_4. Results were read at 600 nm using a BioTek Plate Reader. Standard curves
396 were generated for each assay using a range of HRP-hTf amounts, ranging between 1 x 10^{-3} ng
397 and 2 x 10^{-6} ng. Strains were analyzed in triplicate with standard deviations plotted. Student's *t*
398 test was used to determine significance when compared to the positive control FA6905 (P
399 <0.05).
400 **ICP-MS.** WT and mutant strains were grown under iron-stressed conditions in liquid CDM at
401 36°C with 5% CO_2, as described above. Four hours after dilution to standardized density, 5 µM
402 hTf (30% Fe-saturated) was added for 1 hour. Cells were then pelleted in metal-free tubes at
403 3570 x g for 5 minutes, washed once in 5 mLs of Chelex-treated 10 mM HEPES + 1 mM EDTA
404 (pH 7.4), and washed twice in 5 mLs of 10 mM HEPES (pH 7.4). Digestions and analysis of frozen
405 pellets were performed by University of Georgia's Center for Applied Isotope Studies Plasma
406 Chemistry Laboratory.
407 **Growth in iron-deplete CDM supplemented with hTf.** Strains were plated onto CDM agarose
408 plates supplemented with 2.5 µM hTf (30% Fe-saturated) and incubated for 48 hours at 36°C
409 with 5% CO_2. Images were acquired with Bio-Rad ChemiDoc. For liquid growth assays, strains
410 were plated onto GCB plates supplemented with 10 µM Desferal and incubated at 36°C with 5%
411 CO_2 for 12-16 hours. Iron-starved strains were inoculated into liquid CDM as described above.

412 After doubling, cells were standardized to 2×10^{-5} OD_{600} and plated into 96-well dishes
413 supplemented with 5 µM Desferal and 5 µM hTf. Biotek Synergy and Cytation plate readers
414 were used to incubate the cells at 36°C with 5% CO_2. The OD_{600} was plotted over 24 hours.
415 **Assessment of whole cell binding to hTf in serum.** Strains were grown in liquid CDM as
416 described above. Cells were blocked with 10 mg/mL BSA for 5 minutes after harvest, then cells
417 were incubated with either 1 µM purified hTf or an estimated 1 µM hTf in human serum. Serum
418 hTf was estimated to be approximately 50 µM based on literature and preliminary tests (60-63).
419 Cells were incubated with hTf or serum for 20 minutes at 36°C with 5% CO_2. Lysates were
420 washed twice with 500 µL 1x PBS and standardized and subjected to SDS-PAGE and Western
421 Blotting as described above. Images were acquired with Bio-Rad ChemiDoc.
422 **Molecular dynamic simulations.** The homology model of FA19 TbpA bound to hTf was used as
423 a starting point for simulations. Co-crystallized water molecules as well as the two glycan chains
424 attached to hTf were adopted from the TbpA structure from *N. meningitidis* (PDB 3V8X) (32). A
425 total of three disulfide bonds were formed in TbpA along with 19 in hTf. An outer-membrane
426 model representing that of *N. gonorrhoeae* was created using CHARMM-GUI's Membrane
427 Builder (64) and the TbpA: hTf complex was inserted. The membrane contained 77
428 lipopolysaccharide (LPS) molecules with inner and outer core glycans in the outer leaflet. The
429 inner leaflet contained 174 1-palmitoyl-2-palmitoleoyl-sn-glycero-3-phosphoethanolamine
430 (PYPE), 50 1-palmitoyl-2-palmitoleoyl-sn-glycero-3-phosphoglycerol (PYPG), and 25 1,2-
431 dipalmitoyl-sn-glycero-3-phosphate (DPPA) lipids. A total of 154 Ca2+ and 77 Mg2+ ions were
432 added to neutralize the LPS. An additional 66,164 water molecules as well as 202 K+ and 158
433 Cl− ions were added to solvate the system and bring to a bulk KCl concentration of 150 mM,

434 respectively, using VMD (65). The final system size for the TbpA:hTf system was 290,178 atoms.
435 The apo TbpA system was created from the bound one by deleting hTf, and repeating the
436 solvation and KCl ionization steps. The final system size for the apo TbpA system was 251,845
437 atoms.
438 MD simulations were run using NAMD (66, 67). A 2-fs timestep was used for all simulations with
439 long-range electrostatics calculating every other timestep using the particle-mesh Ewald
440 method (68). A cutoff of 12 Å was used for van der Waals interactions with a force-based
441 switching function beginning at 10 Å. A temperature of 310 K was maintained using Langevin
442 dynamics; for all production simulations, a constant pressure of 1 atm was enforced using an
443 anisotropic Langevin piston. The CHARMM36 force field for lipids and glycans (69, 70) and the
444 CHARMM36m force field for proteins (71) were used. The bound Fe3+ ion and coordinating
445 carbonate ion were covalently bound to one another and additional bonds between Fe3+ and
446 D392, Y426, Y517, and H585 of hTf were added to further enforce coordination as done
447 previously (32). Prior to production runs, the membrane was equilibrated for 50 ns with the
448 protein backbone restrained. In total, four systems with two replicas each were run for 500 ns
449 each (4 µs in aggregate): TbpA (WT) with and without hTf bound as well as TbpA (D355P) with
450 and without hTf bound.
451 **Statistics.** Statistical analyses were conducted by comparing positive control to mutant strains
452 utilizing Student's *t* test. Pairwise differences with a *P* value of <0.05 were considered
453 statistically significant. ELISA and ICP-MS values are shown as the means of multiple
454 concentration points from the studies conducted in at least triplicate ± standard error of the
455 mean. Statistical analysis for hTf-dependent gonococcal growth was completed using PRISM

9.0. A two-way analysis of variance (ANOVA) with Tukey's post-hoc was performed on 3 independent biological replicates. Graph in **FIG 6** shows a representative growth curve.

Acknowledgements

We acknowledge Sarah Jantzi and the University of Georgia Center for Applied Isotope Studies for assistance in development of protocols and analyzing ICP-MS data. This work was supported by funding from the National Health Service grants R01 A1 AI125421, R01 AI125421, R01 AI127793, U19 AI144182, and R01 GM123169. Computational resources were provided through XSEDE (TG-MCB130173), which is supported by the US National Science Foundation (NSF; ACI-1548562). This work also used the Hive cluster, which is supported by the NSF (1828187) and is managed by PACE at Georgia Tech. The funders had no role in study design, data collection, data analysis, decision to publish, or preparation of the manuscript.

468 Figures

469

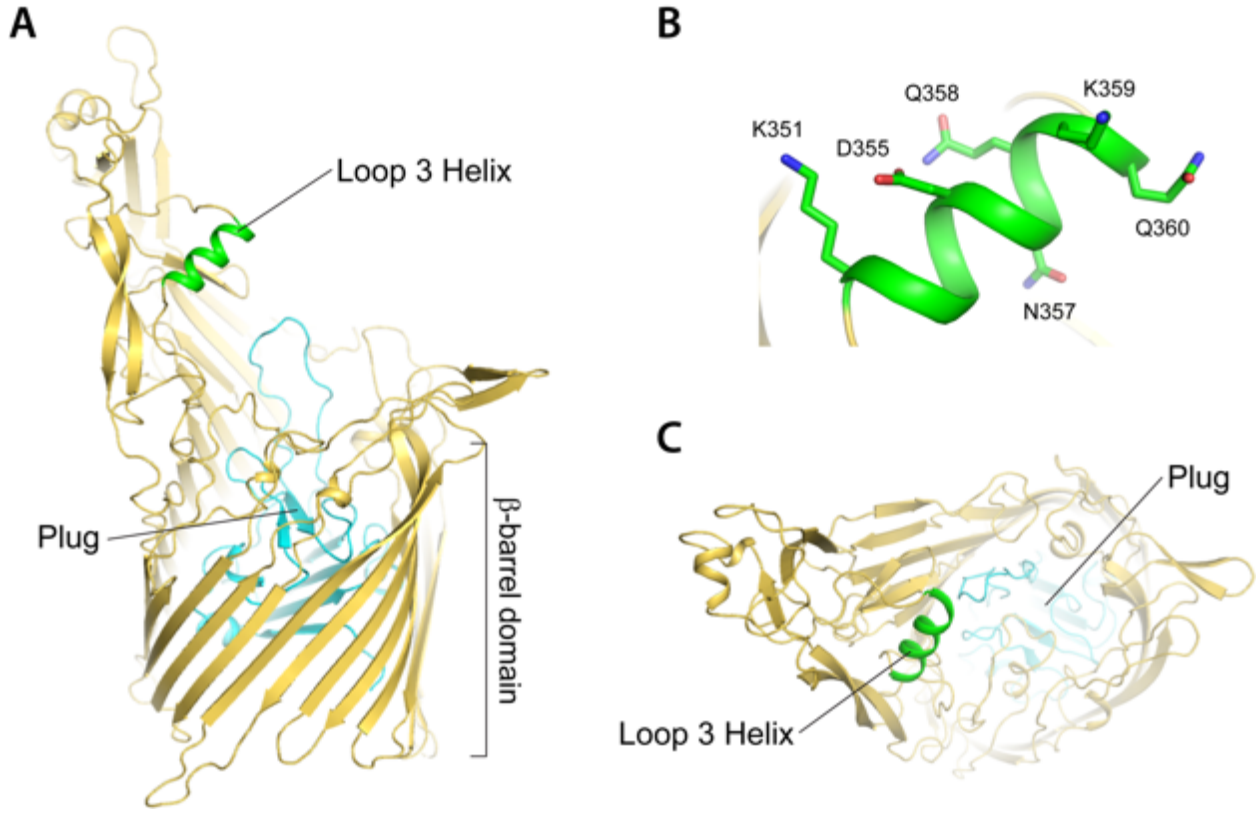

470

471 **FIG 1 TbpA homology model from gonococcal strain FA19**
472 **(A)** TbpA homology model predicted structure based on the *N. meningitidis* strain K454 TbpA
473 crystal structure. The TonB-interacting plug domain is shown in cyan. The L3H is shown in
474 green. **(B)** The residues of the L3H targeted for site-directed mutagenesis in this study. **(C)** A
475 top-down view of TbpA, demonstrating the plug domain situated in the beta-barrel pore.
476

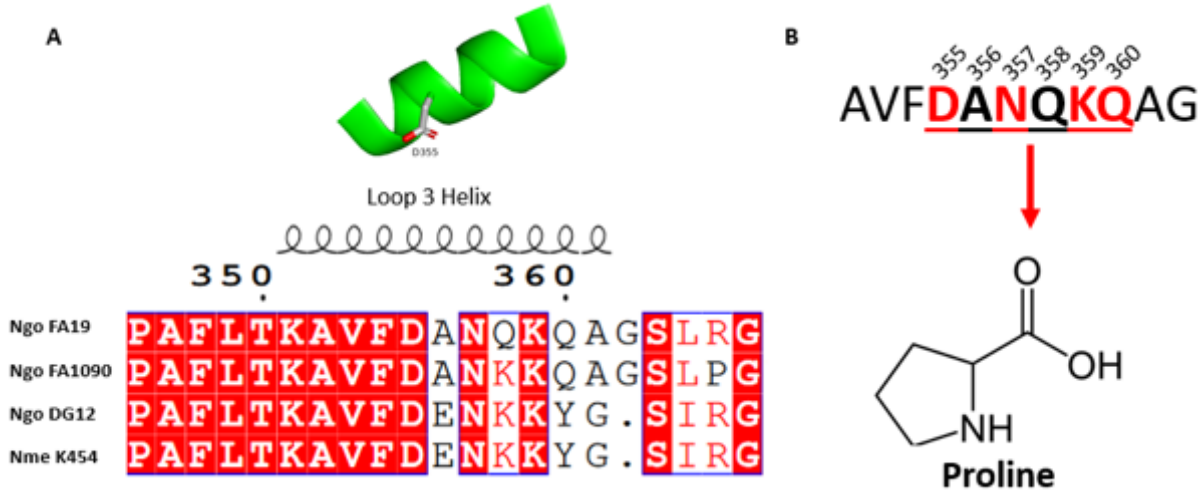

Fig 2 L3H structure and amino acid sequence alignment in *Neisseria* strains.
(A) An alignment of the TbpA L3H domain amino acid sequences for three *N. gonorrhoeae* strains (FA19, FA1090, and DG12) and one *N. meningitidis* strain (K454). Conserved residues are highlighted in red. A secondary structure prediction is shown above the residues. Alignment was generated using ESPript. **(B)** The FA19 TbpA L3H sequence residues that were substituted with proline for this study (D355-Q360). Conserved residues are written in red, and variable residues are shown in black.

485
486
487
488
489
490
491
492
493
494
495
496
497
498
499
500
501
502
503
504

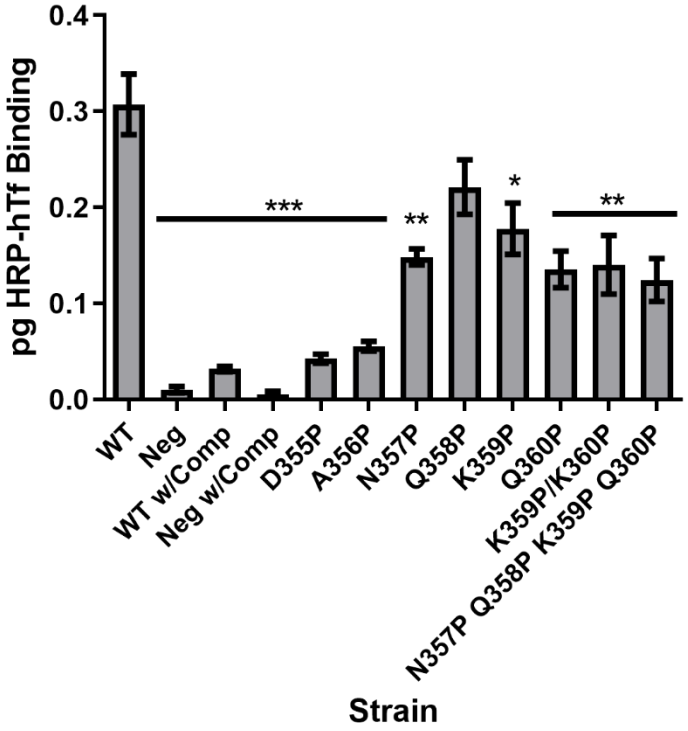

505 **FIG 3 TbpA-hTf binding of *tbpA* mutants in a *tbpB*- background.**
506 Whole, iron-stressed gonococcal cells were applied to microtiter dishes for ELISAs using HRP-
507 labeled hTf as ligand. FA6905 (t*bpA+/tbpB*-) served as the positive control, and FA6815 (t*bpA-*
508 */tbpB*-) and the excess competitor apo-hTf condition (Comp) served as negative controls. The
509 data represent the means ± standard errors of at least three independent experiments. All
510 strains were compared to the positive control FA6905. Statistics were calculated with the
511 Student's *t* test. Significant differences are noted (*P* <0.05 * P <0.005 ** P <0.0005 ***).
512
513

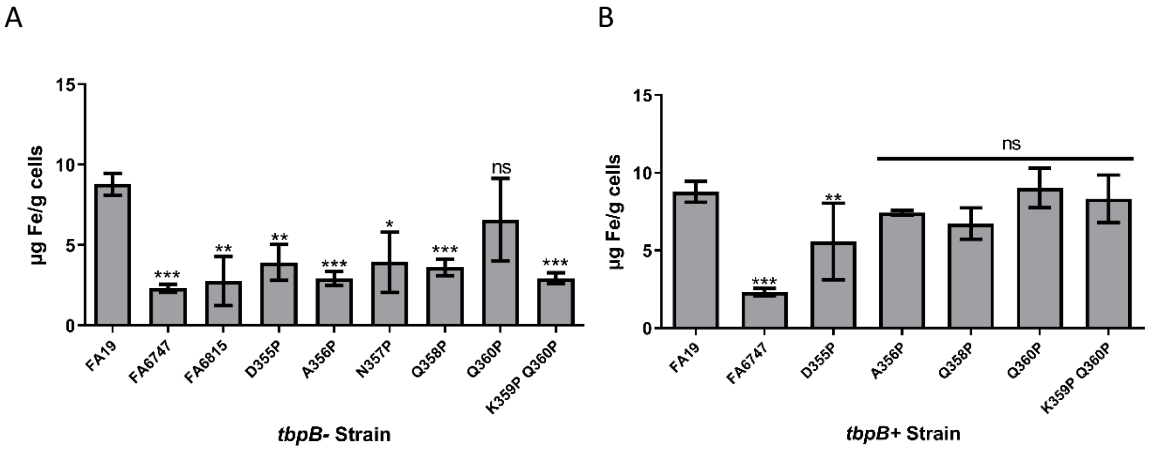

FIG 4 Iron internalization by *tbpA* proline mutants in (A) *tbpB-* background and (B) *tbpB+* background strains.

Gonococcal cells were iron-stressed and allowed to bind to 5 µM 30% Fe-saturated hTf for 1 hour. Bacteria were pelleted and washed prior to being subjected to nitric acid digestion for ICP-MS analysis. Raw µg Fe/g bacteria was plotted for each strain. FA19 (*tbpA+/tbpB+*) served as the positive control. FA6747 (*tbpA-/tbpB+*) served as the negative control. The data represent the means ± standard errors of at least three independent experiments. All strains were compared to the positive control. Statistics were calculated with the Student's *t* test. Non-significant (ns) was defined as p>0.05. Significant differences are noted (P <0.05 * P <0.005 ** P <0.0005 ***).

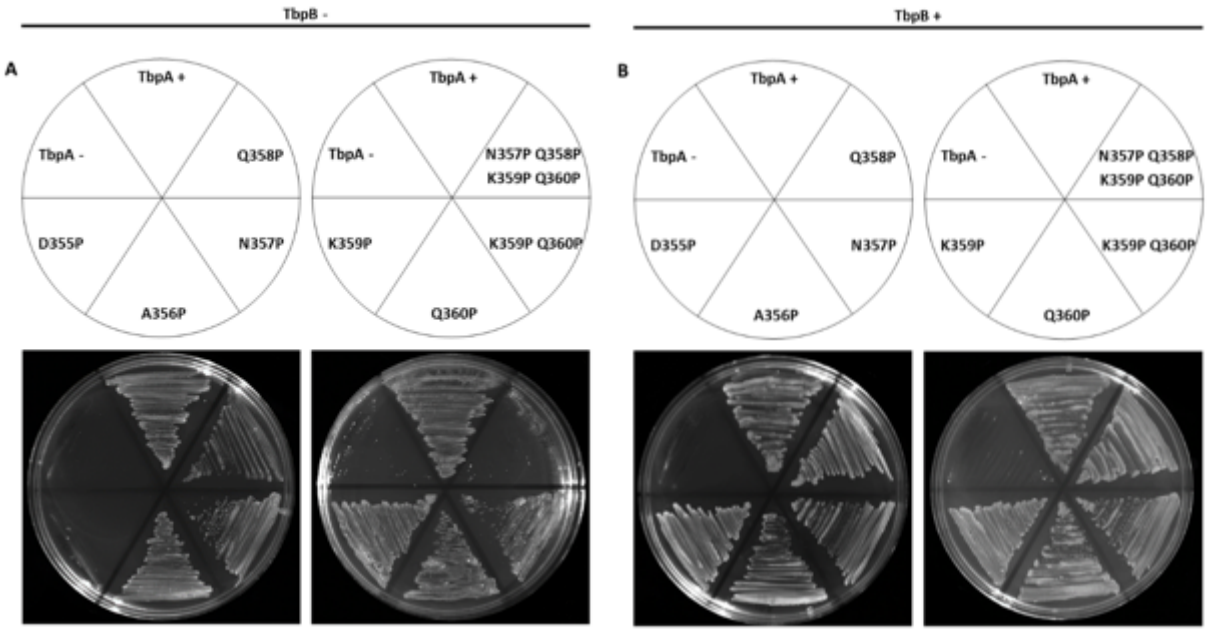

538 **FIG 5 Growth of *tbpA* L3H proline-substitution mutants on hTf plates.**

539 Strains were grown on solid CDM agarose plates supplemented with 30% Fe-saturated hTf as
540 the sole source of iron. CDM agar plates containing 2.5 µM 30% saturated hTf and growth
541 phenotype for **(A)** *tbpB-* background and **(B)** *tbpB+* background. Approximately equivalent
542 amounts of bacteria were applied onto each plate. **(A)** FA6905 (*tbpA+/tbpB-)* served as the
543 positive control for *tbpA tbpB-* mutants, and FA6815 (*tbpA-/tbpB-)* was the negative control for
544 *tbpA tbpB-* mutants. **(B)** FA19 (*tbpA+/tbpB+)* was plated as positive control for *tbpA* mutants in
545 a *tbpB-* background, and FA6747 (*tbpA-/tbpB+)* was the negative control for *tbpA* mutants in
546 the *tbpB+* background.

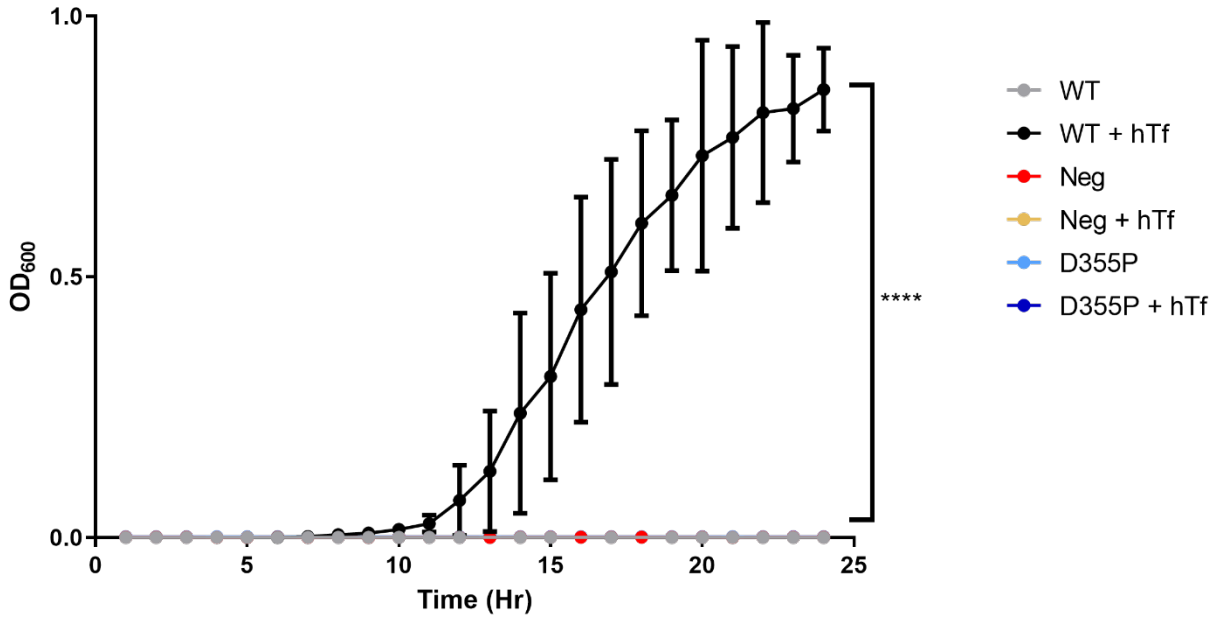

547 **FIG 6 Growth of *tbpA* L3H proline-substitution *tbpB*- mutants on hTf as the sole source of iron**
548 **in liquid CDM.**
549 Whole, iron-stressed gonococci were grown in liquid CDM supplemented with 5 µM 30%
550 saturated hTf over 24 hours. FA6905 (*tbpA+/tbpB-*) was used as a positive control and FA6815
551 (*tbpA-/tbpB-*) served as a negative control. A two-way ANOVA was used to determine
552 significance in comparison to the positive control. Significant differences are noted (P <0.0005
553 ***).
554

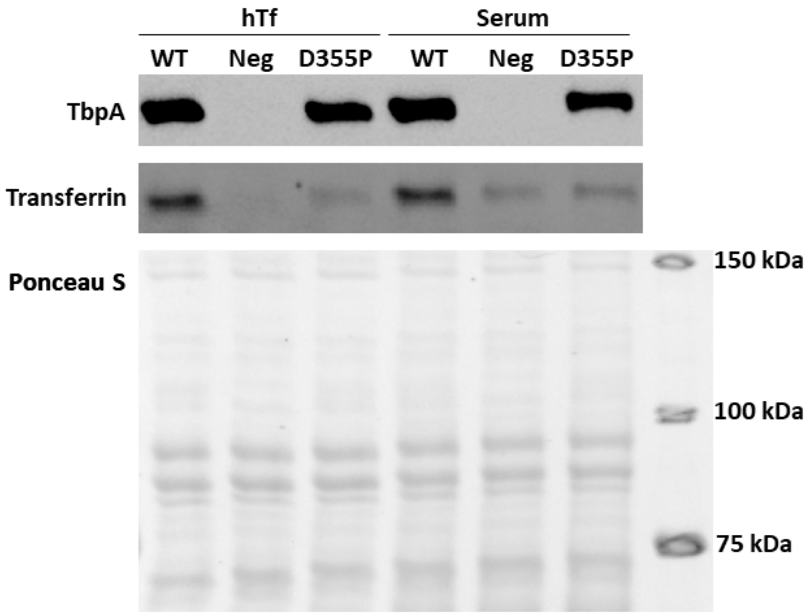

555
556 **FIG 7 The *tbpA* D355P *tbpB*- mutant shows reduced hTf binding compared to FA6905**
557 **(*tbpA+/tbpB-*).**
558 Iron-stressed gonococcal cells were incubated with 1 µM of hTf or approximately 1 µM hTf from
559 human serum for 20 minutes. Lysates were collected and subjected to SDS-PAGE, transferred to
560 nitrocellulose, and probed with polyclonal anti-TbpA antibody and polyclonal anti-hTf antibody.
561 FA6905 (*tbpA+/tbpB-*) was used as a positive control, and FA6815 (*tbpA-/tbpB-*) was used as a
562 negative control. Ponceau S stain was used to show even protein loading. TbpA is
563 approximately 100 kDa, and hTf is approximately 80 kDa.
564

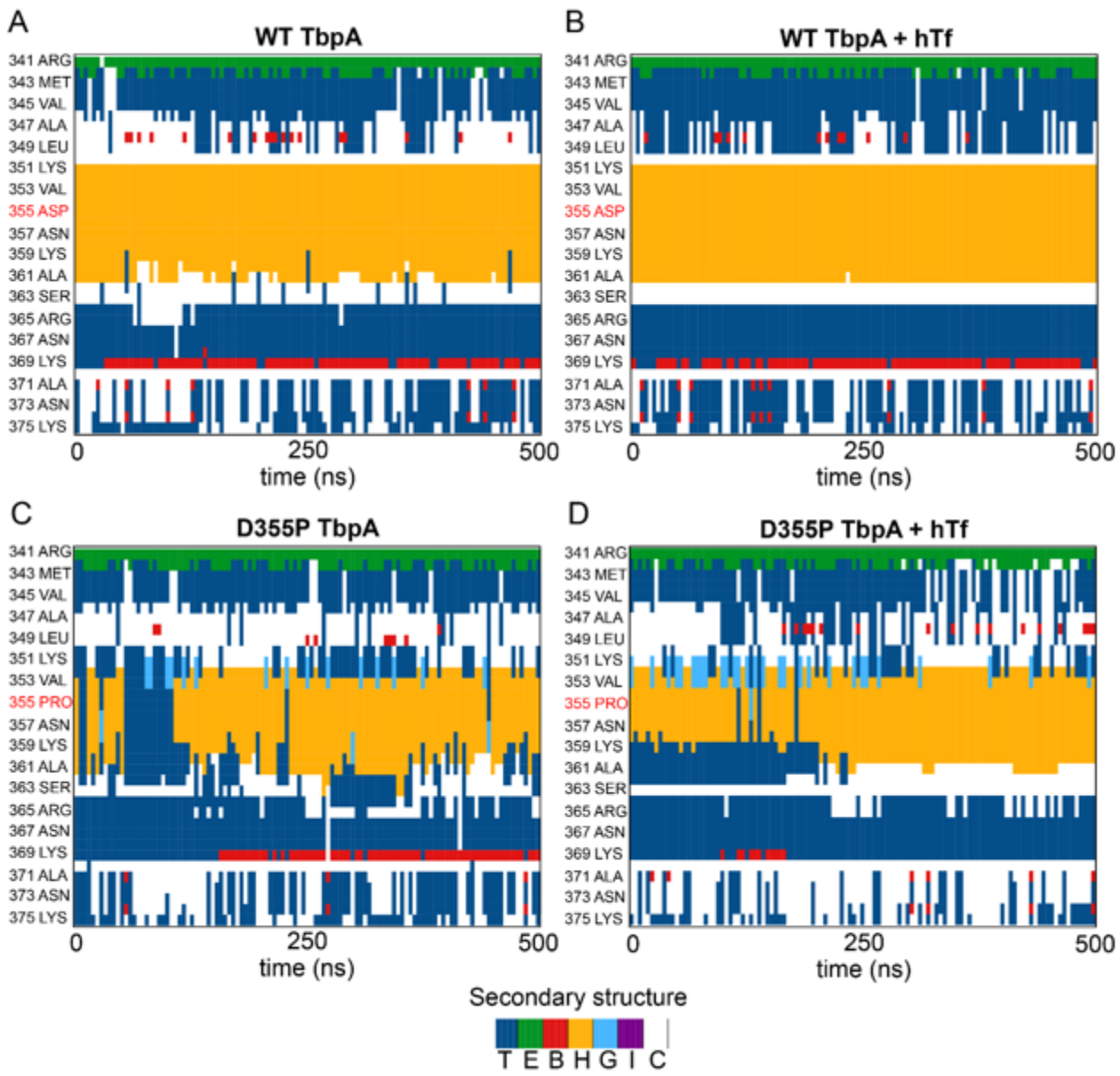

FIG 8 TbpA L3 mutagenesis and secondary structure conservation.

Secondary structure around TbpA L3 over the course of a 500-ns MD simulation for **(A)** WT TbpA, **(B)** WT TbpA +hTf, **(C)** D355P TbpA, and **(D)** D355P TbpA + hTf. The L3H 355 residue is highlighted in red in each panel. The key at the bottom indicates the colors for the seven standard secondary structures as described in the Dictionary of Protein Secondary Structure (72); T is β turn, E is β sheet, B is β bridge, H is α helix, G is 3_{10} helix, I is π helix, and C is unstructured coil. Plots for the second replica are provided in Fig S3 in the Supplemental Information.

576

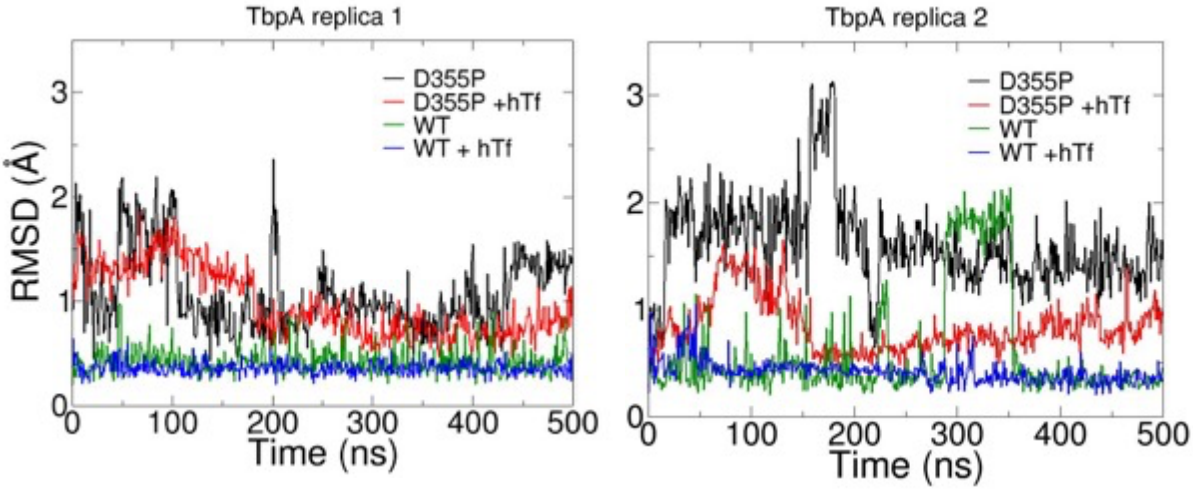

577

578 **FIG 9 RMSD of TbpA L3H mutants bound and unbound to hTf.**

579 Root-mean-square deviation (RMSD) of the L3 helix (residues 351 to 361) after alignment for
580 full-length WT TbpA (green), WT TbpA+ hTf (blue), D355P TbpA (black), and D355P TbpA +hTf
581 (red) over the course of two 500-ns MD simulations (replicas 1, left, and 2, right).

582

583

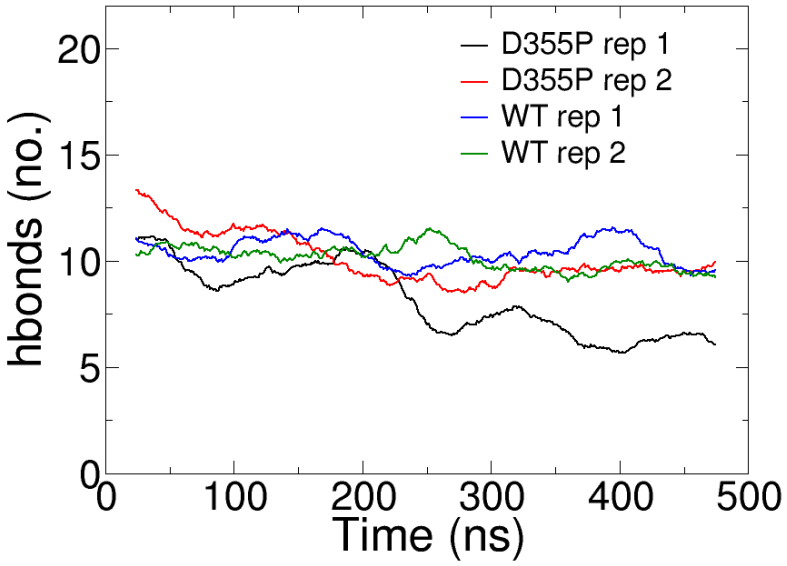

FIG 10 Hydrogen bonds of WT and D355P TbpA over the course of 500ns of MD simulations.

Hydrogen bonds with hTf for WT TbpA (blue and green for replicas 1 and 2, respectively) and TbpA D355P (black and red for replicas 1 and 2) over the course of 500-ns MD simulations.

603

604 **Table 1. Mutagenesis primers used in this study.** Mutations are identified in bold and
605 underline.

Generated Plasmid	Generated TbpA Mutation	Target Plasmid	Primer Name	Direction	5'-3' Sequence	Kit
pGSU001	StuI insert	pUNCH755	oVCU 905	Fwd	GGCAACCACAAATACGG**AGGCCT**GTTTACCAGCGGC	Agilent
			oVCU 906	Rev	GCCGCTGGTAAACAGGCC**TCCGTA**TTTGTGGTTGCC	
pGSU002	D355P	pGSU001	oVCU 927	Fwd	AAGGCGGTTTTT**CCT**GCAAATCAAAAACAGGCG	Agilent
			oVCU 928	Rev	CGCCTGTTTTTGATTTGC**AGG**AAAAACCGCCTT	
pGSU003	A356P	pGSU001	oVCU 929	Fwd	CTGACCAAGGCGGTTTTTGAT**CCA**AATCAAAAACAGGCG	Agilent
			oVCU 930	Rev	CGCCTGTTTTTGATT**TGG**ATCAAAAACCGCCTTGGTCAG	
pGSU004	N357P	pGSU001	oVCU 973	Fwd	TTTTGATGCA**CCT**CAAAAACAGGCGGGTTC	NEB Q5
			oVCU 974	Rev	ACCGCCTTGGTCAGAAAT	
pGSU005	Q358P	pGSU001	oVCU 975	Fwd	TGATGCAAAT**CCA**AAACAGGCGG	NEB Q5
			oVCU 976	Rev	AAAACCGCCTTGGTCAGA	
pGSU006	K359P	pGSU001	oVCU 977	Fwd	TGCAAATCAA**CCA**CAGGCGGGTTC	NEB Q5
			oVCU 978	Rev	TCAAAAACCGCCTTGGTC	
pGSU007	K360P	pGSU001	oVCU 913	Fwd	GATGCAAATCAAAAA**CCG**GCGGGTTCTTTGCGC	Agilent
			oVCU 914	Rev	CTACGTTTAGTTTTT**GGC**CGCCCAAGAAACGCG	
pGSU008	K359P/Q360P	pGSU001	oVCU 917	Fwd	GATGCAAATCAA**CCACCG**GCGGGTTCTTTGCGC	Agilent
			oVCU 918	Rev	CTACGTTTAGTT**GGTGGC**CGCCCAAGAAACGCG	
pGSU009	N357P/Q358P/K359P/Q360P	pGSU008	oVCU 933	Fwd	GCGGTTTTT**CCTCCACCTCCACCACCG**GCGGGTTCTTTGCGC	Agilent
			oVCU 934	Rev	GCGCAAAGAACCCGC**CGGTGGTGGAGGTGGAGG**AAAAACCGC	

606
607

608 **Table 2. Bacterial strains used in this study**

Strain	Description	Source
E. coli		
Top10	F *mcrA* (*mrr-hsdRMS-mcrBC*) 80*lacZ*M15 *lacX74 recA1 deoR araD139* (*ara-leu*)*7697 galU galK rpsL*(Strr) *endA1 nupG*	Invitrogen
XL10 Gold UltraCompetent	*endA1 glnV44 recA1 thi-1 gyrA96 relA1 lac* Hte (*mcrA*)*183* (*mcrCB-hsdSMR-mrr*)*173* Tetr F= [*proAB lacI*q*Z*M15 Tn*10*(Tetr Amyr Cmr)]	Agilent Technologies
NEB 5-alpha Competent	*fhuA2 Δ(argF-lacZ)U169 phoA glnV44 Φ80 Δ(lacZ)M15 gyrA96 recA1 relA1 endA1 thi-1 hsdR17*	New England BioLabs
N. gonorrhoeae		
FA19	wild-type	(73)
FA6747	TbpA- (*tbpA::*mTn3*cat)*	(36, 40)
FA6815	TbpAB- (*ΔtbpB::Ω*)	(38)
FA6905	TbpB- (*ΔtbpB*)	(40)
MCV 192	TbpA L3HΔ (T350-A361)	(25)
RSC 100	TbpA D355P TbpB- (*tbpB*Δ T350-A361)	This study
RSC 101	TbpA D355P	This study
RSC 102	TbpA A356P TbpB- (*tbpB*Δ T350-A361)	This study
RSC 103	TbpA A356P	This study
RSC 104	TbpA N357P TbpB- (*tbpB*Δ T350-A361)	This study
RSC 105	TbpA N357P	This study
RSC 106	TbpA Q358P TbpB- (*tbpB*Δ T350-A361)	This study
RSC 107	TbpA Q358P	This study
RSC 108	TbpA K359P TbpB- (*tbpB*Δ T350-A361)	This study
RSC 109	TbpA K359P	This study
RSC 110	TbpA Q360P TbpB- (*tbpB*Δ T350-A361)	This study
RSC 111	TbpA Q360P	This study
RSC 112	TbpA K369P + Q360P TbpB- (*tbpB*Δ T350-A361)	This study
RSC 113	TbpA K369P + Q360P	This study
RSC 114	TbpA N357P + Q358P + K359P+ Q360P TbpB- (*tbpB*Δ T350-A361)	This study
RSC 115	TbpA N357P + Q358P + K359P + Q360P	This study

609

610

611 **Literature Cited**

612 1. WHO. 2018. Sexually transmitted infections (STIs). https://www.who.int/en/news-room/fact-
613 sheets/detail/sexually-transmitted-infections-(stis).
614 2. CDC. 2021. Incidence, Prevalence and Cost of Sexually Transmitted Infections in the United
615 States. https://www.cdc.gov/nchhstp/newsroom/2021/2018-STI-incidence-prevalence-
616 estimates.html.
617 3. Walker CK, Sweet RL. 2011. Gonorrhea infection in women: prevalence, effects, screening, and
618 management. Int J Womens Health 3:197-206.
619 4. Cornelissen CN, Kelley M, Hobbs MM, Anderson JE, Cannon JG, Cohen MS, Sparling PF. 1998.
620 The transferrin receptor expressed by gonococcal strain FA1090 is required for the experimental
621 infection of human male volunteers. Mol Microbiol 27:611-6.
622 5. Schmidt KA, Schneider H, Lindstrom JA, Boslego JW, Warren RA, Van de Verg L, Deal CD, McClain
623 JB, Griffiss JM. 2001. Experimental gonococcal urethritis and reinfection with homologous
624 gonococci in male volunteers. Sex Transm Dis 28:555-64.
625 6. Unemo M, Shafer WM. 2014. Antimicrobial resistance in *Neisseria gonorrhoeae* in the 21st
626 century: past, evolution, and future. Clin Microbiol Rev 27:587-613.
627 7. Portnoy J, Mendelson J, Clecner B, Heisler L. 1974. Asymptomatic gonorrhea in the male. Can
628 Med Assoc J 110:169 passim.
629 8. Liu Y, Liu W, Russell MW. 2014. Suppression of host adaptive immune responses by *Neisseria*
630 *gonorrhoeae*: role of interleukin 10 and type 1 regulatory T cells. Mucosal Immunol 7:165-76.
631 9. Liu Y, Feinen B, Russell MW. 2011. New concepts in immunity to *Neisseria gonorrhoeae*: innate
632 responses and suppression of adaptive immunity favor the pathogen, not the host. Front
633 Microbiol 2:52.
634 10. WHO. 2018. WHO Gonococcal AMR Surveillance Programme.
635 https://www.who.int/data/gho/data/themes/topics/who-gonococcal-amr-surveillance-
636 programme-who-gasp.
637 11. Ohnishi M, Golparian D, Shimuta K, Saika T, Hoshina S, Iwasaku K, Nakayama S, Kitawaki J,
638 Unemo M. 2011. Is *Neisseria gonorrhoeae* initiating a future era of untreatable gonorrhea?:
639 detailed characterization of the first strain with high-level resistance to ceftriaxone. Antimicrob
640 Agents Chemother 55:3538-45.
641 12. Unemo M, Golparian D, Nicholas R, Ohnishi M, Gallay A, Sednaoui P. 2012. High-level cefixime-
642 and ceftriaxone-resistant *Neisseria gonorrhoeae* in France: novel *penA* mosaic allele in a
643 successful international clone causes treatment failure. Antimicrob Agents Chemother 56:1273-
644 80.
645 13. Lahra MM, Ryder N, Whiley DM. 2014. A new multidrug-resistant strain of *Neisseria*
646 *gonorrhoeae* in Australia. N Engl J Med 371:1850-1.
647 14. Cámara J, Serra J, Ayats J, Bastida T, Carnicer-Pont D, Andreu A, Ardanuy C. 2012. Molecular
648 characterization of two high-level ceftriaxone-resistant *Neisseria gonorrhoeae* isolates detected
649 in Catalonia, Spain. J Antimicrob Chemother 67:1858-60.
650 15. Fifer H, Livermore DM, Uthayakumaran T, Woodford N, Cole MJ. 2021. What's left in the
651 cupboard? Older antimicrobials for treating gonorrhoea. J Antimicrob Chemother
652 doi:10.1093/jac/dkaa559.
653 16. Yan J, Chen Y, Yang F, Ling X, Jiang S, Zhao F, Yu Y, van der Veen S. 2021. High percentage of the
654 ceftriaxone-resistant *Neisseria gonorrhoeae* FC428 clone among isolates from a single hospital in
655 Hangzhou, China. J Antimicrob Chemother doi:10.1093/jac/dkaa526.
656 17. Sancta St. Cyr MLB, MD1,2; Kimberly A. Workowski, MD1,3; Laura H. Bachmann, MD1; Cau
657 Pham, PhD1; Karen Schlanger, PhD1; Elizabeth Torrone, PhD1; Hillard Weinstock, MD1; Ellen N.
658 Kersh, PhD1; Phoebe Thorpe, MD. 2020. Update to CDC's Treatment Guidelines for Gonococcal

659 Infection, 2020. Prevention UDoHaHSCfDCa, Morbidity and Mortality Weekly Report.
660 http://dx.doi.org/10.15585/mmwr.mm6950a6.
661 18. Virji M. 2009. Pathogenic neisseriae: surface modulation, pathogenesis and infection control.
662 Nat Rev Microbiol 7:274-86.
663 19. Zhu W, Chen CJ, Thomas CE, Anderson JE, Jerse AE, Sparling PF. 2011. Vaccines for gonorrhea:
664 can we rise to the challenge? Front Microbiol 2:124.
665 20. Russell MW, Jerse AE, Gray-Owen SD. 2019. Progress Toward a Gonococcal Vaccine: The Way
666 Forward. Front Immunol 10:2417.
667 21. Criss AK, Kline KA, Seifert HS. 2005. The frequency and rate of pilin antigenic variation in
668 *Neisseria gonorrhoeae*. Mol Microbiol 58:510-9.
669 22. Cornelissen CN. 2008. Identification and characterization of gonococcal iron transport systems
670 as potential vaccine antigens. Future Microbiol 3:287-98.
671 23. Martínez-Martínez S, Frandoloso R, Rodríguez-Ferri E-F, García-Iglesias M-J, Pérez-Martínez C,
672 Álvarez-Estrada Á, Gutiérrez-Martín C-B. 2016. A vaccine based on a mutant transferrin binding
673 protein B of *Haemophilus parasuis* induces a strong T-helper 2 response and bacterial clearance
674 after experimental infection. Veterinary Immunology and Immunopathology 179:18-25.
675 24. Martinez-Martinez S, Frandoloso R, Gutierrez-Martin CB, Lampreave F, Garcia-Iglesias MJ, Perez-
676 Martinez C, Rodriguez-Ferri EF. 2011. Acute phase protein concentrations in colostrum-deprived
677 pigs immunized with subunit and commercial vaccines against Glässer's disease. Vet Immunol
678 Immunopathol 144:61-7.
679 25. Cash DR, Noinaj N, Buchanan SK, Cornelissen CN. 2015. Beyond the Crystal Structure: Insight
680 into the Function and Vaccine Potential of TbpA Expressed by *Neisseria gonorrhoeae*. Infect
681 Immun 83:4438-49.
682 26. Chan C, Andisi VF, Ng D, Ostan N, Yunker WK, Schryvers AB. 2018. Are lactoferrin receptors in
683 Gram-negative bacteria viable vaccine targets? Biometals 31:381-398.
684 27. Martinez-Martinez S, Rodriguez-Ferri EF, Frandoloso R, Garrido-Pavon JJ, Zaldivar-Lopez S,
685 Barreiro C, Gutierrez-Martin CB. 2016. Molecular analysis of lungs from pigs immunized with a
686 mutant transferrin binding protein B-based vaccine and challenged with *Haemophilus parasuis*.
687 Comp Immunol Microbiol Infect Dis 48:69-78.
688 28. Frandoloso R, Martinez-Martinez S, Calmettes C, Fegan J, Costa E, Curran D, Yu RH, Gutierrez-
689 Martin CB, Rodriguez-Ferri EF, Moraes TF, Schryvers AB. 2015. Nonbinding site-directed mutants
690 of transferrin binding protein B exhibit enhanced immunogenicity and protective capabilities.
691 Infect Immun 83:1030-8.
692 29. Noinaj N, Buchanan SK, Cornelissen CN. 2012. The transferrin-iron import system from
693 pathogenic *Neisseria* species. Mol Microbiol 86:246-57.
694 30. Price GA, Hobbs MM, Cornelissen CN. 2004. Immunogenicity of gonococcal transferrin binding
695 proteins during natural infections. Infect Immun 72:277-83.
696 31. Cornelissen CN, Anderson JE, Boulton IC, Sparling PF. 2000. Antigenic and sequence diversity in
697 gonococcal transferrin-binding protein A. Infect Immun 68:4725-35.
698 32. Noinaj N, Easley NC, Oke M, Mizuno N, Gumbart J, Boura E, Steere AN, Zak O, Aisen P,
699 Tajkhorshid E, Evans RW, Gorringe AR, Mason AB, Steven AC, Buchanan SK. 2012. Structural
700 basis for iron piracy by pathogenic *Neisseria*. Nature 483:53-8.
701 33. Noinaj N, Gumbart JC, Buchanan SK. 2017. The beta-barrel assembly machinery in motion. Nat
702 Rev Microbiol 15:197-204.
703 34. Noinaj N, Buchanan SK. 2014. Structural insights into the transport of small molecules across
704 membranes. Curr Opin Struct Biol 27:8-15.
705 35. Noinaj N, Guillier M, Barnard TJ, Buchanan SK. 2010. TonB-dependent transporters: regulation,
706 structure, and function. Annu Rev Microbiol 64:43-60.

707 36. Cornelissen CN, Biswas GD, Tsai J, Paruchuri DK, Thompson SA, Sparling PF. 1992. Gonococcal
708 transferrin-binding protein 1 is required for transferrin utilization and is homologous to TonB-
709 dependent outer membrane receptors. J Bacteriol 174:5788-97.
710 37. Irwin SW, Averil N, Cheng CY, Schryvers AB. 1993. Preparation and analysis of isogenic mutants
711 in the transferrin receptor protein genes, *tbpA* and *tbpB*, from *Neisseria meningitidis*. Mol
712 Microbiol 8:1125-33.
713 38. Anderson JE, Sparling PF, Cornelissen CN. 1994. Gonococcal transferrin-binding protein 2
714 facilitates but is not essential for transferrin utilization. J Bacteriol 176:3162-70.
715 39. Renauld-Mongenie G, Poncet D, Mignon M, Fraysse S, Chabanel C, Danve B, Krell T, Quentin-
716 Millet MJ. 2004. Role of transferrin receptor from a *Neisseria meningitidis tbpB* isotype II strain
717 in human transferrin binding and virulence. Infect Immun 72:3461-70.
718 40. Cornelissen CN, Sparling PF. 1996. Binding and surface exposure characteristics of the
719 gonococcal transferrin receptor are dependent on both transferrin-binding proteins. J Bacteriol
720 178:1437-44.
721 41. Retzer MD, Yu R, Zhang Y, Gonzalez GC, Schryvers AB. 1998. Discrimination between apo and
722 iron-loaded forms of transferrin by transferrin binding protein B and its N-terminal subfragment.
723 Microb Pathog 25:175-80.
724 42. Duran GN, Özbil M. 2021. Structural rearrangement of *Neisseria meningitidis* transferrin binding
725 protein A (TbpA) prior to human transferrin protein (hTf) binding. Turk J Chem 45:1146-1154.
726 43. Steere AN, Miller BF, Roberts SE, Byrne SL, Chasteen ND, Smith VC, MacGillivray RT, Mason AB.
727 2012. Ionic residues of human serum transferrin affect binding to the transferrin receptor and
728 iron release. Biochemistry 51:686-94.
729 44. Pogoutse AK, Moraes TF. 2017. Iron acquisition through the bacterial transferrin receptor. Crit
730 Rev Biochem Mol Biol 52:314-326.
731 45. Yost-Daljev MK, Cornelissen CN. 2004. Determination of surface-exposed, functional domains of
732 gonococcal transferrin-binding protein A. Infect Immun 72:1775-85.
733 46. Beernink PT, Shaughnessy J, Braga EM, Liu Q, Rice PA, Ram S, Granoff DM. 2011. A
734 meningococcal factor H binding protein mutant that eliminates factor H binding enhances
735 protective antibody responses to vaccination. J Immunol 186:3606-14.
736 47. Calmettes C, Alcantara J, Yu RH, Schryvers AB, Moraes TF. 2012. The structural basis of
737 transferrin sequestration by transferrin-binding protein B. Nat Struct Mol Biol 19:358-60.
738 48. Yadav R, Noinaj N, Ostan N, Moraes T, Stoudenmire J, Maurakis S, Cornelissen CN. 2019.
739 Structural Basis for Evasion of Nutritional Immunity by the Pathogenic *Neisseriae*. Front
740 Microbiol 10:2981.
741 49. Boulton IC, Yost MK, Anderson JE, Cornelissen CN. 2000. Identification of discrete domains
742 within gonococcal transferrin-binding protein A that are necessary for ligand binding and iron
743 uptake functions. Infect Immun 68:6988-96.
744 50. Cornelissen CN. 2003. Transferrin-iron uptake by Gram-negative bacteria. Front Biosci 8:d836-
745 47.
746 51. Kenney CD, Cornelissen CN. 2002. Demonstration and characterization of a specific interaction
747 between gonococcal transferrin binding protein A and TonB. J Bacteriol 184:6138-45.
748 52. West D, Reddin K, Matheson M, Heath R, Funnell S, Hudson M, Robinson A, Gorringe A. 2001.
749 Recombinant *Neisseria meningitidis* transferrin binding protein A protects against experimental
750 meningococcal infection. Infect Immun 69:1561-7.
751 53. Price GA, Russell MW, Cornelissen CN. 2005. Intranasal administration of recombinant *Neisseria*
752 *gonorrhoeae* transferrin binding proteins A and B conjugated to the cholera toxin B subunit
753 induces systemic and vaginal antibodies in mice. Infect Immun 73:3945-53.

754 54. Cornelissen CN, Anderson JE, Sparling PF. 1997. Characterization of the diversity and the
755 transferrin-binding domain of gonococcal transferrin-binding protein 2. Infect Immun 65:822-8.
756 55. Rossi R, Granoff DM, Beernink PT. 2013. Meningococcal factor H-binding protein vaccines with
757 decreased binding to human complement factor H have enhanced immunogenicity in human
758 factor H transgenic mice. Vaccine 31:5451-7.
759 56. Kellogg DS, Jr., Peacock WL, Jr., Deacon WE, Brown L, Pirkle DI. 1963. *Neisseria gonorrhoeae*.
760 Virulence Genetically Linked to Clonal Variation. J Bacteriol 85:1274-9.
761 57. West SE, Sparling PF. 1987. Aerobactin utilization by *Neisseria gonorrhoeae* and cloning of a
762 genomic DNA fragment that complements *Escherichia coli fhuB* mutations. J Bacteriol 169:3414-
763 21.
764 58. Robert X, Gouet P. 2014. Deciphering key features in protein structures with the new ENDscript
765 server. Nucleic Acids Res 42:W320-4.
766 59. Maurakis S, Keller K, Maxwell CN, Pereira K, Chazin WJ, Criss AK, Cornelissen CN. 2019. The novel
767 interaction between *Neisseria gonorrhoeae* TdfJ and human S100A7 allows gonococci to subvert
768 host zinc restriction. PLoS Pathog 15:e1007937.
769 60. Kasvosve I, Delanghe J. 2002. Total iron binding capacity and transferrin concentration in the
770 assessment of iron status. Clin Chem Lab Med 40:1014-8.
771 61. Page MGP. 2019. The Role of Iron and Siderophores in Infection, and the Development of
772 Siderophore Antibiotics. Clin Infect Dis 69:S529-s537.
773 62. Ganz T, Nemeth E. 2015. Iron homeostasis in host defence and inflammation. Nat Rev Immunol
774 15:500-10.
775 63. Andrews NC, Ganz T. 2019. The molecular basis of iron metabolism
776 doi:10.1002/9781119252863.ch13, p 161-172. Oxford, UK: John Wiley & Sons, Ltd, Oxford, UK.
777 64. Wu EL, Cheng X, Jo S, Rui H, Song KC, Dávila-Contreras EM, Qi Y, Lee J, Monje-Galvan V, Venable
778 RM, Klauda JB, Im W. 2014. CHARMM-GUI Membrane Builder toward realistic biological
779 membrane simulations. J Comput Chem 35:1997-2004.
780 65. Humphrey W, Dalke A, Schulten K. 1996. VMD – Visual Molecular Dynamics. J Mol Graphics
781 14:33-38.
782 66. Phillips JC, Braun R, Wang W, Gumbart J, Tajkhorshid E, Villa E, Chipot C, D. Skeel R, Kale L,
783 Schulten K. 2005. Scalable molecular dynamics with NAMD. J Comput Chem 26:1781-1802.
784 67. Phillips JC, Hardy DJ, Maia JDC, Stone JE, Ribeiro JV, Bernardi RC, Buch R, Fiorin G, Hénin J, Jiang
785 W, McGreevy R, Melo MCR, Radak BK, Skeel RD, Singharoy A, Wang Y, Roux B, Aksimentiev A,
786 Luthey-Schulten Z, Kale L, Schulten K, Chipot C, Tajkhorshid E. 2020. Scalable molecular
787 dynamics on CPU and GPU architectures with NAMD. J Chem Phys 153:044130.
788 68. Darden TA, York DM, Pedersen LG. 1993. Particle mesh Ewald: An N log N method for Ewald
789 sums in large systems. J Comput Phys 98:10089-10092.
790 69. Klauda JB, Venable RM, Freites JA, O'Connor JW, Tobias DJ, Mondragon-Ramirez C, Vorobyov I,
791 MacKerell Jr. AD, Pastor RW. 2010. Update of the CHARMM all-atom additive force field for
792 lipids: validation on six lipid types. J Phys Chem B 114:7830-7843.
793 70. Guvench O, Hatcher ER, Venable RM, Pastor RW, MacKerell Jr. AD. 2009. Additive empirical
794 CHARMM force field for glycosyl linked hexopyranoses. JCTC 5:2353-2370.
795 71. Huang J, Rauscher S, Nawrocki G, Ran T, Feig M, de Groot BL, Grubmüller H, MacKerell Jr. AD.
796 2017. CHARMM36m: an improved force field for folded and intrinsically disordered proteins.
797 Nat Methods 14:71-73.
798 72. Kabsch W, Sander C. 1983. Dictionary of protein secondary structure: pattern recognition of
799 hydrogen-bonded and geometrical features. Biopolymers 22:2577-637.

800 73. Mickelsen PA, Sparling PF. 1981. Ability of *Neisseria gonorrhoeae*, *Neisseria meningitidis*, and
801 commensal *Neisseria* species to obtain iron from transferrin and iron compounds. Infect Immun
802 33:555-64.

803